Article



# Complexation-Induced Reduction of $Cu^{II}$ to $Cu^{I}$ Promoted by a Distorted Tetrahedral $N_4$-Type Schiff-Base Ligand

Tomoyuki Takeyama * , Daisuke Shirabe , Nobutsugu Hamamoto , Takehiro Ohta

Posted Date: 27 August 2025

doi: 10.20944/preprints202508.1982.v1

Keywords: copper; metal complex; reduction; ligand; electronic structure

 doi:10.20944/preprints202508.1982.v1



*Article*

# Complexation-Induced Reduction of $Cu^{II}$ to $Cu^{I}$ Promoted by a Distorted Tetrahedral $N_4$-Type Schiff-Base Ligand

**Tomoyuki Takeyama *, Daisuke Shirabe, Nobutsugu Hamamoto and Takehiro Ohta**

Department of Applied Chemistry, Sanyo-Onoda City University, 1-1-1, Daigaku-dori, Sanyo-Onoda, Yamaguchi 756-0884, Japan

* Correspondence: takeyama.t@rs.socu.ac.jp; takeyama.t@rs.socu.ac.jp;

**Abstract**

Although spontaneous or complexation-induced reductions of $Cu^{II}$ to $Cu^{I}$ have occasionally been observed, controlling these processes remains a challenge. Herein, we report the synthesis of $Cu^{I}$ complexes via the complexation-induced reduction of $Cu^{II}$ complexes with pyridine-containing $N_4$ Schiff-base ligand **L** incorporating a biphenyl unit (**L** = *N*,*N*′-([1,1′-biphenyl]-2,2′-diyl)bis(1-(6-methylpyridin-2-yl)methanimine)). Such a reduction has not yet been observed in previously reported $Cu^{II}$ complexes with pyridine-containing $N_4$ Schiff-base ligands, strongly suggesting that the torsional distortion of the ligand framework induced by the biphenyl moiety effectively promotes the complexation-induced reduction of $Cu^{II}$ to $Cu^{I}$. The $Cu^{I}$ complexes were thoroughly characterized by $^1$H NMR spectroscopy, UV–vis–NIR spectroscopy, and single-crystal X-ray diffraction analyses. The $[Cu^{I}(\mathbf{L})]^+$ complex undergoes a reversible redox process with its oxidized species, which was identified as a $Cu^{II}$ complex based on spectroelectrochemical measurements and theoretical calculations.

**Keywords:** copper; metal complex; reduction; ligand; electronic structure

## 1. Introduction

The redox reaction of copper (Cu) complexes plays a key role in many biological systems [1–4]. Notably, blue Cu proteins such as plastocyanin and azurin function as biological electron carriers by virtue of the redox reactions between $Cu^{I}$ and $Cu^{II}$ at their active sites [1,2]. To achieve a rapid and reversible redox process between $Cu^{I}$ and $Cu^{II}$, the coordination geometry must remain nearly unchanged throughout the redox event. However, the preferred coordination geometry of $Cu^{I}$ and $Cu^{II}$ complexes differs considerably owing to their distinct electronic configuration. Specifically, $Cu^{I}$ adopts a tetrahedral coordination geometry due to its closed-shell $d^{10}$ configuration, whereas the $d^9$ configuration and characteristic Jahn–Teller distortion of $Cu^{II}$ result in square-planar or distorted square-pyramidal complexes. Therefore, an appropriate ligand design is essential in order to control the redox properties and oxidation states of Cu complexes.

Cu complexes exhibit a rich redox chemistry, which can sometimes complicate the control of their oxidation states. For instance, several studies have reported the formation of $Cu^{I}$ complexes from $Cu^{II}$ precursors even in the absence of reducing agents [5–10]. Such a reduction, which is commonly termed spontaneous or complexation-induced reduction [6–10], can be triggered by an intramolecular electron transfer from the ligand [8,10] or by the participation of solvents such as alcohols [5]. The spontaneous or complexation-induced reduction of $Cu^{II}$ complexes often occurs unintentionally, and limited efforts have so far been devoted to deliberately controlling this process [5–10]. Nevertheless, understanding and controlling the geometric preferences of both $Cu^{I}$ and $Cu^{II}$ may enable the deliberate induction of complexation-induced reduction.

 doi:10.20944/preprints202508.1982.v1



Pyridine-based nitrogen ligands are widely used in Cu complexes due to their strong coordination ability with both $Cu^{I}$ and $Cu^{II}$ oxidation states [11–20]. We envisioned that incorporating a biphenyl moiety into the pyridine-based ligand framework of $Cu^{II}$ complexes could promote their complexation-induced reduction. The biphenyl unit consists of two aromatic rings with a dihedral angle of ~42° between them, which introduces a remarkable torsional distortion [6]. Such a torsional distortion could facilitate the complexation-induced reduction of $Cu^{II}$ by favoring the formation of the tetrahedral geometry, which is energetically preferred in $Cu^{I}$ complexes. To test our hypothesis, we designed biphenyl-bridged pyridine-containing $N_4$ Schiff-base ligand **L** (Figure 1).

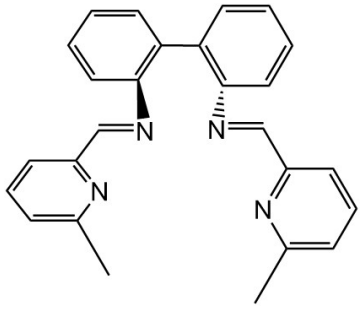


**Figure 1.** Structure of ligand **L** prepared in this study.

Herein, we report the design of ligand **L** and its reaction with a $Cu^{II}$ precursor to yield a $Cu^{I}$ complex via complexation-induced reduction. In addition, we discuss the effect of the biphenyl unit on the complexation-induced reduction of $Cu^{II}$ on the basis of a comparison with other Cu complexes bearing pyridine-containing $N_4$ Schiff-base ligands.

## 2. Results and Discussion

Tetradentate ligand **L** was synthesized via the condensation reaction between 6-methyl-2-pyridinecarboxaldehyde and 2,2′-diaminobiphenyl in ethanol. Interestingly, the reaction of **L** with $Cu^{II}(CF_3SO_3)_2$ immediately furnished a black-green suspension and induced the spontaneous reduction of the $Cu^{II}$ center to $Cu^{I}$. Recrystallization of the $Cu^{I}$ complex using DMF and diethyl ether afforded deep-green crystals, which were subjected to a single-crystal X-ray diffraction (XRD) analysis. The resulting molecular structure is shown in Figure 2(a). The presence of two Cu centers and two $CF_3SO_3^-$ counter anions in the asymmetric unit indicates that the oxidation state of Cu is +I. The resulting molecular structure shows that the molecular formula of the obtained $Cu^{I}$ complex is $[Cu^{I}_2(\mathbf{L})_2](CF_3SO_3)_2$. The bond distances between Cu and the pyridine N ($N_{py}$) are 2.097–2.114 Å, i.e., slightly shorter than those between Cu and the imine N ($N_{im}$) (2.055–2.074 Å). The $N_{im}$–Cu–$N_{py}$ bond angles (80.9°–81.7°) are considerably smaller than the $N_{py}$–Cu–$N_{py}$ (97.2°–97.7°) and $N_{im}$–Cu–$N_{im}$ (144.2°–144.6°) bond angles. The dihedral angles between the N(1)–Cu(1)–N(2) and N(5)–Cu(1)–N(6) planes as well as between the N(3)–Cu(2)–N(4) and N(7)–Cu(2)–N(8) planes are 78.81° and 77.66°, respectively. Considering that the ideal square-planar and tetrahedral geometries are characterized by dihedral angles of 0° and 90°, respectively, the obtained values suggest that the coordination geometries of the Cu(1) and Cu(2) centers are slightly distorted from the ideal tetrahedral coordination geometry.

 doi:10.20944/preprints202508.1982.v1



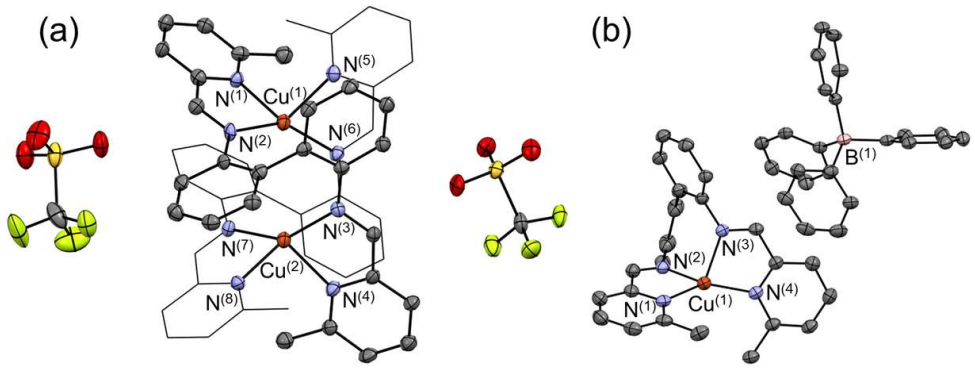


**Figure 2.** Molecular structures of (a) $[Cu^{I}_2(\mathbf{L})_2](CF_3SO_3)_2$ and (b) $[Cu^{I}(\mathbf{L})]BPh_4$ in the crystalline state with thermal ellipsoids at 50% probability; all hydrogen atoms are omitted for clarity.

The reaction of **L** with $Cu^{II}(ClO_4)_2{\cdot}6H_2O$ also immediately furnished a dark-green suspension. The resulting solid was dissolved in acetonitrile, subjected to counter-anion exchange via the reaction with 10 equivalents of $NaBPh_4$, and recrystallized into black crystals. The corresponding single-crystal XRD analysis provided the molecular structure shown in Figure 2(b). In contrast to $[Cu^{I}_2(\mathbf{L})_2](CF_3SO_3)_2$, the asymmetric unit contains only one Cu center and one $BPh_4^-$ anion, revealing that the molecular formula of the obtained Cu complex is $[Cu(\mathbf{L})]BPh_4$. Considering the charge balance of $[Cu(\mathbf{L})]BPh_4$, the oxidation state of Cu can also be assigned as +I. Therefore, the reaction between **L** and a $Cu^{II}$ source produced $Cu^{I}$ complexes regardless of the counter anion. However, mononuclear or dinuclear $Cu^{I}$ complexes were obtained depending on the counter anion.

The Cu–$N_{py}$ bond lengths in $[Cu^{I}(\mathbf{L})]BPh_4$ are 1.985 and 2.027 Å, which are by 0.06–0.13 Å shorter than those of $[Cu^{I}_2(\mathbf{L})_2](CF_3SO_3)_2$ (2.097–2.114 Å). In contrast, the length of the Cu–$N_{im}$ bonds in $[Cu^{I}(\mathbf{L})]BPh_4$ (2.053 and 2.100 Å) are comparable to those in $[Cu^{I}_2(\mathbf{L})_2](CF_3SO_3)_2$ (2.055–2.074 Å). The $N_{py}(1)$–Cu–$N_{py}(4)$ bond angle (135.27°) is significantly larger than the $N_{py}$–Cu–$N_{im}$ (81.26° and 81.38°) and $N_{im}$–Cu–$N_{im}$ (88.93°) bond angles. The dihedral angle between the N(1)–Cu(1)–N(2) and N(3)–Cu(1)–N(4) planes (63.30°) is slightly smaller than the corresponding angles in $[Cu^{I}_2(\mathbf{L})_2](CF_3SO_3)_2$. These results indicate that $[Cu^{I}(\mathbf{L})]BPh_4$ possesses a distorted tetrahedral coordination geometry.

The $[Cu^{I}_2(\mathbf{L})_2](CF_3SO_3)_2$ and $[Cu^{I}(\mathbf{L})]BPh_4$ complexes are EPR silent (Figure 3(a)), indicating that they are diamagnetic species with a Cu oxidation state of +I. The $^1$H NMR spectra of $[Cu^{I}_2(\mathbf{L})_2](CF_3SO_3)_2$ and $[Cu^{I}(\mathbf{L})]BPh_4$ in acetonitrile-$d_3$ are quite similar to each other (Figures S1-2). All $^1$H NMR signals originating from the pyridine moieties in $[Cu^{I}(\mathbf{L})]BPh_4$ are very slightly high-field shifted (~0.01 ppm) compared to the corresponding signals of $[Cu^{I}_2(\mathbf{L})_2](CF_3SO_3)_2$ (Figure S2). Overall, the EPR and $^1$H NMR spectroscopy results show no clear difference between mononuclear and dinuclear complexes. In contrast, the UV–vis–NIR spectrum of $[Cu^{I}_2(\mathbf{L})_2](CF_3SO_3)_2$ in acetonitrile clearly differs from that of $[Cu^{I}(\mathbf{L})]BPh_4$. As shown in Figure 3(b), the UV–vis–NIR spectrum of $[Cu^{I}_2(\mathbf{L})_2](CF_3SO_3)_2$ shows a shoulder band at 450 nm ($\varepsilon$ = 3000 $M^{-1}{\cdot}cm^{-1}$) and a low-intensity band at 590 nm ($\varepsilon$ = 700 $M^{-1}{\cdot}cm^{-1}$), while the corresponding spectrum of $[Cu^{I}(\mathbf{L})]BPh_4$ exhibits an intense band at 450 nm ($\varepsilon$ = 5000 $M^{-1}{\cdot}cm^{-1}$) and a low-intensity band at 585 nm ($\varepsilon$ = 1500 $M^{-1}{\cdot}cm^{-1}$).

 doi:10.20944/preprints202508.1982.v1



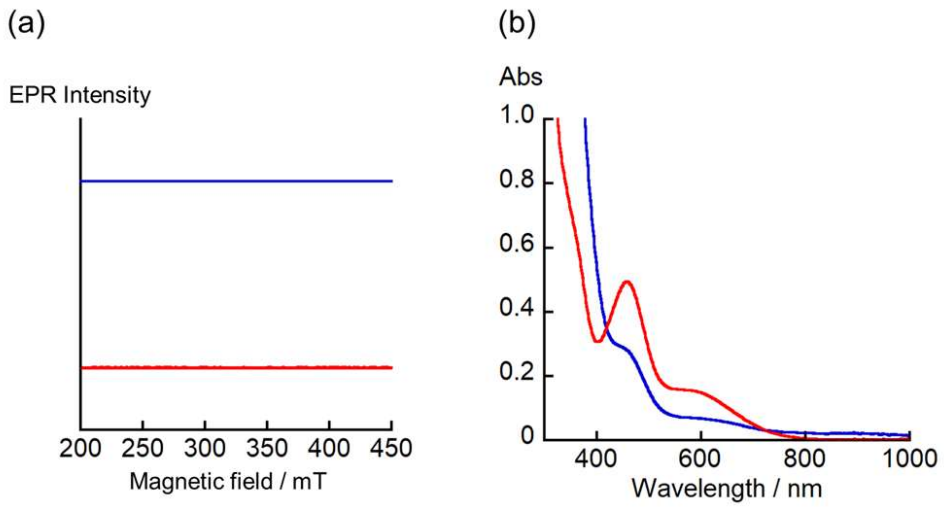


**Figure 3.** (a) Solid-state EPR spectra and (b) UV–vis–NIR spectra of $[Cu^{I}_2(\mathbf{L})_2](CF_3SO_3)_2$ (blue) and $[Cu^{I}(\mathbf{L})]BPh_4$ (red) in acetonitrile.

Considering that various $Cu^{II}$ complexes have been synthesized by mixing a $Cu^{II}$ source and organic Schiff-base ligands [4,21–25], the formation of the $Cu^{I}$ complexes $[Cu^{I}_2(\mathbf{L})_2](CF_3SO_3)_2$ and $[Cu^{I}(\mathbf{L})]BPh_4$ via the reaction between a $Cu^{II}$ source and **L** in the absence of additional reductants is unusual. Although the complexation-induced reduction of $Cu^{II}$ has been previously reported, the reductant has not been unequivocally characterized in most cases [6,7,9].

To clarify why the $Cu^{I}$ complex is formed by simply mixing $Cu^{II}$ ions and **L**, we investigated the redox behavior of $[Cu(\mathbf{L})]BPh_4$. The cyclic voltammogram of $[Cu^{I}(\mathbf{L})]BPh_4$ shows one reversible redox couple and one irreversible oxidation peak (Figure 4). The irreversible oxidation peak at 0.42 V vs. $Fc^{+/0}$ is also observed in the cyclic voltammogram of $NaBPh_4$ in acetonitrile, but not in that of $[Cu^{I}_2(\mathbf{L})_2](CF_3SO_3)_2$ (Figure S3). Therefore, it can be attributed to the oxidation of $BPh_4^-$. The $E^{\circ\prime}$ value of the reversible redox event was estimated to be 0.05 V vs. $Fc^{+/0}$. To determine the electron stoichiometry ($n$) of the reversible redox processes observed for $[Cu^{I}(\mathbf{L})]BPh_4$, spectroelectrochemical measurements were conducted by recording the UV–vis–NIR spectra of $[Cu^{I}(\mathbf{L})]BPh_4$ in acetonitrile at varying applied potentials between −0.13 and 0.11 V vs. $Fc^{+/0}$ (Figure 5(a)).

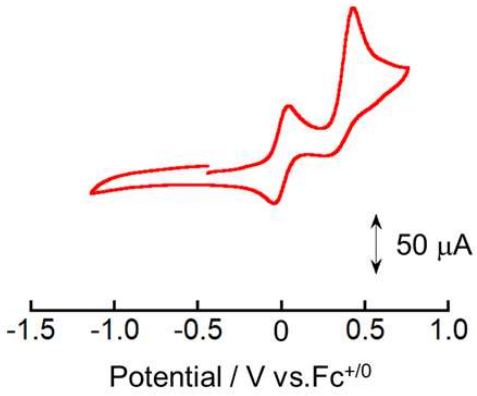


**Figure 4.** Cyclic voltammogram of $[Cu^{I}(\mathbf{L})]BPh_4$ in acetonitrile (supporting electrolyte: 0.1 M $TBAPF_6$; scan rate (v): 100 $mV{\cdot}s^{-1}$).

 doi:10.20944/preprints202508.1982.v1



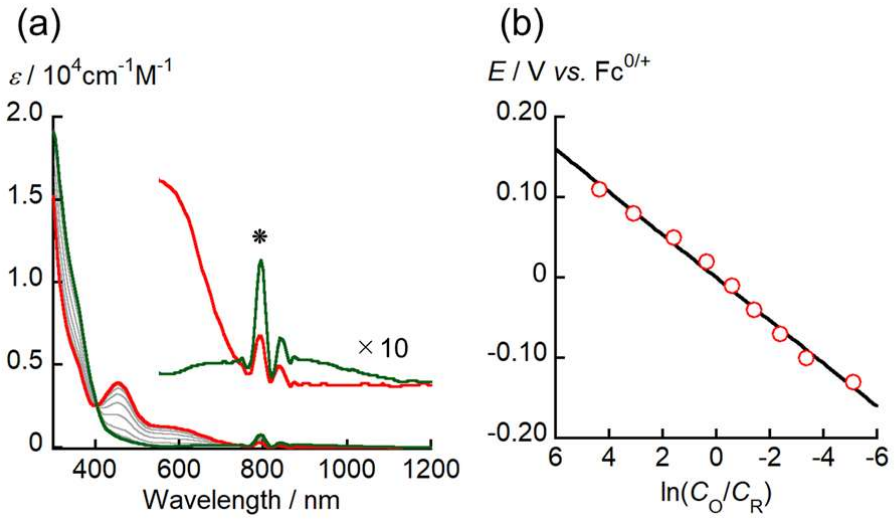


**Figure 5.** (a) UV–vis–NIR spectral change during the electrochemical oxidation of [Cu$^{I}$(**L**)]BPh$_4$ recorded at varying applied potentials from −0.13 to 0.11 V vs. Fc$^{+/0}$ (potential increments: 0.03 V) in acetonitrile (supporting electrolyte: 0.1 M TBAPF$_6$; $T$ = 295 K). The red and green bold curves are the absorption spectra of [Cu$^{I}$(**L**)]BPh$_4$ and [Cu(**L**)]$^{2+}$, respectively. (b) Nernstian plot calculated from the absorbance at 460 nm.

As a general trend, the intensity of the absorption bands at ~453 and 530–720 nm decreases with decreasing applied potentials, while new absorption bands appear at ~350 and ~800 nm. The presence of isosbestic points was clearly observed at ~402 and ~730 nm, indicating that a redox equilibrium of [Cu$^{I}$(**L**)]BPh$_4$ solely occurred in this potential range. The spectral change of [Cu$^{I}$(**L**)]BPh$_4$ converged at 0.11 V vs. Fc$^{+/0}$, implying that the oxidation of [Cu$^{I}$(**L**)]BPh$_4$ was complete at this potential. The ratio between the concentrations of the oxidant ($C_O$) and the [Cu$^{I}$(**L**)]BPh$_4$ reductant ([Cu$^{I}$(**L**)]BPh$_4$, $C_R$) at each potential was calculated using the absorbance change. Figure 5(b) shows the relationship between ln($C_O$/$C_R$) and the applied potential ($E$ vs. Fc$^{+/0}$), which should theoretically follow the Nernst equation (eq 1):

$$E = E^{\circ\prime} + (RT/nF)\ln(C_O/C_R), \quad (1)$$

where $R$, $T$, and $F$ are the gas constant (8.314 J·mol$^{-1}$·K$^{-1}$), the absolute temperature (295 K), and the Faraday constant (96485 C·mol$^{-1}$), respectively. The $n$ and $E^{\circ\prime}$ values for the redox reaction of [Cu$^{I}$(**L**)]BPh$_4$ were determined to be 0.98(4) and 0.00(1) V vs. Fc$^{+/0}$, respectively, by least-squares fitting eq 1 to the plot of $E$ as a function of ln($C_O$/$C_R$) (Figure 5(b)). This result suggests that the redox reactions of [Cu$^{I}$(**L**)]BPh$_4$ are single-electron processes. In addition, the $E^{\circ\prime}$ value is consistent within an acceptable margin of error with the redox potential determined via CV.

To elucidate the electronic structure of the electrochemically generated one-electron oxidized complex [Cu(**L**)]$^{2+}$, we measured its EPR spectrum at 77 K. Axial signals typical for mononuclear Cu$^{II}$ systems ($g_1$ = 2.25 and $g_2$ = 2.10) were observed (Figure 6), suggesting that the one-electron oxidation of [Cu$^{I}$(**L**)]$^{+}$ could provide a Cu$^{II}$ complex. However, the EPR spectral features of [Cu(**L**)]$^{2+}$ are more similar to those observed for distorted square-planar Cu$^{II}$ complexes [23] than to those of tetrahedral Cu$^{II}$ complexes [26,27]. These results suggest that the oxidation from [Cu$^{I}$(**L**)]$^{+}$ to [Cu(**L**)]$^{2+}$ is accompanied by a structural change toward a more planar coordination geometry.

 doi:10.20944/preprints202508.1982.v1



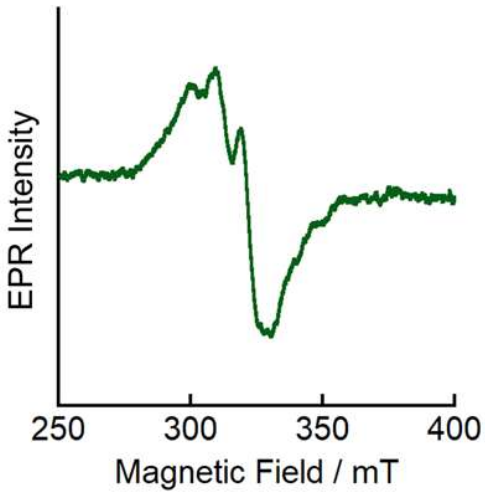


**Figure 6.** EPR spectrum of electrochemically generated $[Cu(\mathbf{L})]^{2+}$ in acetonitrile (supporting electrolyte: 0.1 M $TBAPF_6$; $T$ = 77 K). Experimental conditions: [complex] = 10 mM; frequency: 9.4354 GHz; microwave power: 7 mW; modulation amplitude: 0.05 mT.

Next, to test the validity of our hypothesis, we performed density-functional-theory (DFT) and time-dependent DFT (TD-DFT) calculations on $[Cu^{I}(\mathbf{L})]^{+}$ and $[Cu(\mathbf{L})]^{2+}$. The corresponding DFT-optimized structures are shown in Figure S4, and selected structural parameters are summarized in Table S1.

The bond lengths between the Cu center and the imino N in $[Cu(\mathbf{L})]^{2+}$, i.e., Cu(1)–N(2) and Cu(1)–N(3) (1.994 Å), are ~0.13 Å shorter than those of $[Cu^{I}(\mathbf{L})]^{+}$ (Cu(1)–N(2) = 2.116 Å; Cu(1)–N(3) = 2.122 Å). This suggests that the increase in the positive charge of Cu through the oxidation from $[Cu^{I}(\mathbf{L})]^{+}$ to $[Cu(\mathbf{L})]^{2+}$ strengthens these coordination bonds. To discuss the structural change upon oxidation from $[Cu^{I}(\mathbf{L})]^{+}$ to $[Cu(\mathbf{L})]^{2+}$, we focused on the dihedral angles between the N(1)–Cu(1)–N(2) and N(3)–Cu(1)–N(4) planes in both complexes. The dihedral angle of DFT-optimized $[Cu^{I}(\mathbf{L})]^{+}$ (64.36°) (Figure S5) is in good agreement with the XRD value (63.30°). In contrast, the dihedral angle of DFT-optimized $[Cu(\mathbf{L})]^{2+}$ exhibits a considerably smaller value (56.04°). These results indicate that oxidation is accompanied by a structural change toward a more planar coordination geometry. The spin-density plot of $[Cu(\mathbf{L})]^{2+}$ clearly shows that the unpaired electron is mainly distributed on the Cu center and the coordinated N atoms (Figure 7). In addition, the total spin-density value of Cu and N (0.98) indicates that Cu has a $3d^9$ electron configuration, i.e., the most common state of $Cu^{II}$ complexes.

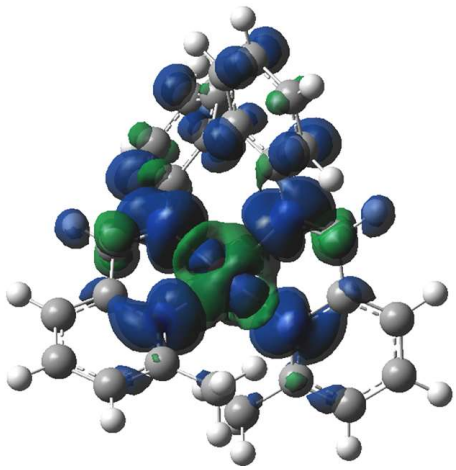

 doi:10.20944/preprints202508.1982.v1



**Figure 7.** Spin-density plot of $[Cu(\mathbf{L})]^{2+}$; the blue and green for the positive and negative spin densities, respectively. Spin-density values: Cu(1) = 0.58, N(1) = 0.13, N(2) = 0.07, N(3) = 0.07, and N(4) = 0.13.

Using the DFT-optimized structure, we estimated the electronic absorption spectra of $[Cu^{I}(\mathbf{L})]^{+}$ and $[Cu(\mathbf{L})]^{2+}$ by TD-DFT calculations (Figure 8). The TD-DFT calculations reproduced the experimental spectral features well but underestimated the transition energies. Several intense bands of $[Cu^{I}(\mathbf{L})]^{+}$ between 415 and 770 nm are attributable to the charge transfer from Cu to the ligand (MLCT). These MLCT bands significantly decreased upon the one-electron oxidation of $[Cu^{I}(\mathbf{L})]^{+}$, while a new absorption band attributed to the charge transfer from **L** to Cu (LMCT) appeared at ~830 $cm^{-1}$. Consequently, $[Cu(\mathbf{L})]^{2+}$ can be categorized as a $Cu^{II}$ complex ($[Cu^{II}(\mathbf{L})]^{2+}$).

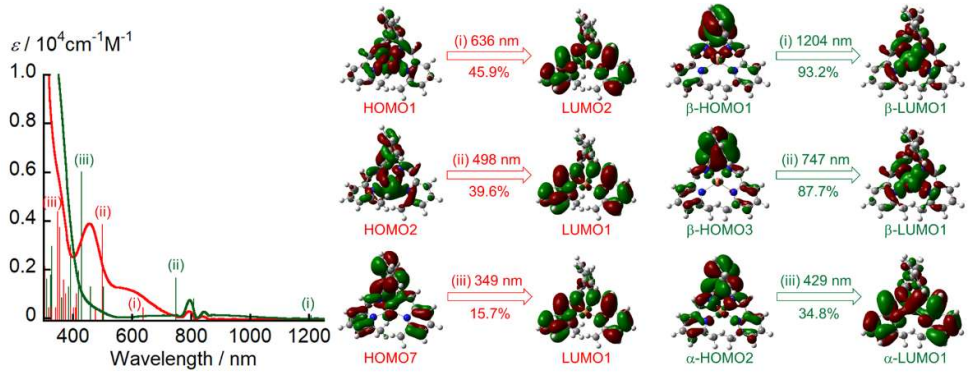


**Figure 8.** UV–vis–NIR spectra of $[Cu^{I}(\mathbf{L})]^{+}$ (red line) and $[Cu(\mathbf{L})]^{2+}$ (green line) in pyridine and band positions and intensities predicted by TD-DFT calculations. The vertical red and green lines indicate the calculated transitions for $[Cu^{I}(\mathbf{L})]^{+}$ and $[Cu(\mathbf{L})]^{2+}$, respectively. The main contributing charge transfers for each absorption including the involved orbitals, are depicted as well.

Isolating the oxidized complex $[Cu^{II}(\mathbf{L})]^{2+}$ would provide valuable information to clarify the complexation-induced reduction of $Cu^{II}$ to $Cu^{I}$. However, the electrochemically generated $[Cu^{II}(\mathbf{L})]^{2+}$ gradually decomposed once the electrolysis was stopped. Unfortunately, attempts to synthesize and isolate $[Cu^{II}(\mathbf{L})]^{2+}$ via chemical oxidation of $[Cu^{I}(\mathbf{L})]^{+}$ proved unsuccessful.

Regardless, we were also interested in identifying the reducing agent responsible for the reduction of $Cu^{II}$. In some of the previous studies on the complexation-induced reduction of $Cu^{II}$ to $Cu^{I}$ [5–10], ethanol, which was used as the reaction solvent, was identified as the reducing agent [5,8,10]. Initially, we hypothesized that this could be also the case in the present study. However, $[Cu^{I}(\mathbf{L})]BPh_4$ was successfully synthesized in the absence of ethanol (for details, see the Supporting Information) both under ambient conditions and a $N_2$ atmosphere. These results suggest that neither the solvent nor the atmosphere gas is involved in the reduction of $Cu^{II}$.

The $[Cu^{I}(\mathbf{L})]BPh_4$ complex was synthesized in a yield of approximately 45%, which was consistently reproduced across multiple experiments. Given that the yield remained relatively low despite the reproducibility, we hypothesized that ligand **L** or its precursors (6-methyl-2-pyridinecarboxaldehyde and 2,2′-diaminobiphenyl) might be involved in the complexation-induced reduction of $Cu^{II}$ during complex formation. To examine this hypothesis, the complex was synthesized using a slight excess of either 6-methyl-2-pyridinecarboxaldehyde or 2,2′-diaminobiphenyl relative to the stoichiometric ratio. However, the yield of the complex remained in the range of 45%–48% (for details, see the Supporting Information) without significant improvement. In contrast, when two equivalents of **L** were reacted with the $Cu^{II}$ source, the yield of $[Cu^{I}(\mathbf{L})]BPh_4$ increased to 70% (for details, see the Supporting Information). This result suggests that uncoordinated **L** may participate in the reduction of $Cu^{II}$ to $Cu^{I}$. To gain a better understanding of this reduction process, we made extensive efforts to identify the byproducts. However, the formation of multiple decomposition products hindered their identification.

 doi:10.20944/preprints202508.1982.v1



Previously, Fabbrizzi and co-workers have synthesized various $Cu^{II}$ complexes with pyridine-containing $N_4$ Schiff-base ligands (Figure S6) by mixing a $Cu^{II}$ source with the corresponding ligands [21]. Specifically, they employed Schiff-base ligands derived from two 6-methyl-2-carboxypyridine moieties bridged by ethylenediamine or 1,2-cyclohexanediamine [21]. These ligand frameworks possess relatively high planarity. In fact, the dihedral angles between the N(1)–Cu(1)–N(2) and N(3)–Cu(1)–N(4) planes in the $Cu^{II}$ complex (~22°) [21] is significantly smaller than that of $[Cu^{II}(\mathbf{L})]^{2+}$ (56.04°). At present, we hypothesize that such a difference in dihedral angle may play a key role in the reduction of $Cu^{II}$ to $Cu^{I}$. The torsion of **L** induced by the biphenyl moiety may favor the formation of the tetrahedral geometry preferred by $Cu^{I}$ complexes over the coordination to $Cu^{II}$. Therefore, approaching a four-coordinated tetrahedral coordination geometry around the Cu center would facilitate the reduction of $Cu^{II}$ to $Cu^{I}$ during complexation. According to Shimazaki and co-workers, modification of the coordination geometry in Cu–phenolate complexes from a trigonal-bipyramidal to a tetrahedral four-coordinate structure induces a change in the electronic structure from a $Cu^{II}$–(phenolate) species to a $Cu^{I}$–(phenoxyl radical) species [4,28]. This distortion of the coordination geometry around the Cu center facilitates the intramolecular electron transfer from the coordinating phenolate to the $Cu^{II}$ ion, resulting in the formation of the $Cu^{I}$–(phenoxyl radical) species. The fate of the oxidation state of the metal center in a Cu complex is sometimes governed by its coordination structure.

## 3. Materials and Methods

*Materials*

All chemicals used in this work were of reagent grade and used as received, unless otherwise specified.

***Caution!*** *Although there were no incidents in our laboratory, transition-metal perchlorates may explode violently. They should be prepared only in small quantities and handled with the utmost care.*

*Synthesis of $Cu^{I}$ Complexes*

**$[Cu_2(L)_2](CF_3SO_3)_2$.** A solution of 6-methyl-2-pyridinecarboxaldehyde (52.6 mg, 0.434 mmol) and 2,2′-diaminobiphenyl (40.0 mg, 0.217 mmol) in ethanol (0.5 mL) was slowly treated with $Cu^{II}(CF_3SO_3)_2$ (80.0 mg, 0.221 mmol) in ethanol (0.5 mL), and the resulting mixture was stirred for 1 h. The green precipitate formed was collected by filtration, dissolved in a mixture of DMF (200 μL) and ethanol (800 μL), and recrystallized into deep-green crystals via vapor diffusion with diethyl ether. Yield: 35 mg (13%). $^1$H NMR (399.78 MHz, acetonitrile-$d_3$, $\delta$ / ppm vs. TMS): 2.61 (s, 12H, –C$H_3$), 7.17 (d, 4H, aryl, $J_{H–H}$ = 7.6 Hz), 7.32–7.46 (m, 12H, aryl) 7.72 (dd, 8H, py, $J_{H–H}$ = 18.6 Hz, $J_{H–H}$ = 7.6 Hz), 8.02 (t, 4H, py, $J_{H–H}$ = 8.0 Hz), 8.56 (s, 4H, –C*H*=N–).

**$[Cu(L)]BPh_4$.** A solution of 6-methyl-2-pyridinecarboxaldehyde (26.0 mg, 0.215 mmol) and 2,2′-diaminobiphenyl (20.0 mg, 0.109 mmol) in ethanol (1 mL) was slowly treated with $Cu^{II}(ClO_4)_2{\cdot}6H_2O$ (40.6 mg, 0.110 mmol) in ethanol (1 mL), and the mixture was stirred for 1 h. The resulting precipitate was collected by filtration and dissolved in acetonitrile. $NaBPh_4$ (0.35 g, 1.02 mmol) was added to this solution, and the mixture was stirred for several minutes. The mixture was then concentrated under reduced pressure, and ethanol (1 mL) was added to the residue to yield a black solid, which was collected by filtration, dissolved in a mixture of DMF (200 μL) and ethanol (800 μL), and recrystallized into black crystals via vapor diffusion with diethyl ether. Yield: 31 mg (37%). $^1$H NMR (399.78 MHz, acetonitrile-$d_3$, $\delta$ / ppm vs. TMS): 2.60 (s, 6H, –C$H_3$), 6.84 (t, 4H, –B–Ph$_4$, $J_{H–H}$ = 7.2 Hz), 6.99 (t, 8H, –B–Ph$_4$, $J_{H–H}$ = 7.2 Hz), 7.17 (d, 2H, aryl, $J_{H–H}$ = 8.0 Hz), 7.27 (m, 8H, –B–Ph$_4$), 7.31–7.46 (m, 6H, aryl), 7.71 (dd, 4H, py, $J_{H–H}$ = 18.0 Hz, $J_{H–H}$ = 8.0 Hz), 8.02 (t, 2H, py, $J_{H–H}$ = 7.6 Hz), 8.55 (s, 2H, –C*H*=N–).

*Physical Measurements*

 doi:10.20944/preprints202508.1982.v1



The $^1$H NMR spectra were recorded on a JEOL ECX-400 NMR spectrometer ($^1$H: 399.78 MHz). Chemical shifts are referenced to TMS ($\delta$ = 0 ppm). CV measurements were performed on the Cu$^{I}$ complexes (1.00 mM) dissolved in acetonitrile containing 0.1 M *tetra-n*-butylammonium hexafluorophosphate perchlorate ($TBAPF_6$) at 295 K under a dry Ar atmosphere using an Autolab NOVA 2 electrochemical analyzer. A three-electrode system consisting of a GC disk working electrode, a Pt wire counter electrode, and a $Ag^{0/+}$ reference electrode (0.1 M TBAP + 1 mM $AgNO_3/CH_3CN$) was employed. The ferrocene/ferrocenium ion redox couple ($Fc^{0/+}$) was used as the external standard redox system. All samples were prepared under an inert Ar atmosphere. Dissolved $O_2$ in the sample solutions was removed by purging with Ar gas for at least 10 min prior to starting the experiments.

UV–vis–NIR spectroelectrochemical measurements of Cu$^{I}$ complexes in acetonitrile were performed with a HITACHI UH4150 spectrophotometer equipped with an optically transparent thin layer electrode (OTTLE) cell at 295 K [29,30]. The optical path length was calibrated spectrophotometrically ($1.0 \times 10^{-2}$ cm) [29,30]. The three-electrode system was the same as that in the aforementioned electrochemical experiments except that the working electrode was a Pt gauze (80 mesh). The potential applied on OTTLE was controlled using Autolab NOVA 2. The absorption spectrum at each potential step was recorded after equilibration of the electrochemical reaction at the applied potential on the working electrode, which was completed within 3 min. The sample solution in the OTTLE cell was prepared in a similar manner to that for the electrochemical measurements.

*Crystallographic Analysis*

XRD data for $[Cu_2(\mathbf{L})_2](CF_3SO_3)_2$ and $[Cu(\mathbf{L})]BPh_4$ were collected on a Rigaku XtaLab Synergy-R-DW-TT diffractometer equipped with a hybrid pixel array detector and graphite-monochromated Cu $K\alpha$ ($\lambda$ = 1.54184 Å) radiation at 100 K. The sample was mounted on a MiTeGen Dual Thickness MicroMount and placed in a temperature-controlled $N_2$ gas flow. Intensity data were collected by taking oscillation photographs. Reflection data were corrected for both Lorentz and polarization effects. The structures were solved using direct methods and refined anisotropically using the SHELX program suite [31] for non-hydrogen atoms via full-matrix least-squares calculations. Each refinement was continued until all shifts were smaller than one-third of the standard deviation of the parameters involved. Hydrogen atoms were placed at calculated positions. All calculations were performed using the crystallographic software package *Olex2* [32].

Crystallographic data for $[Cu_2(\mathbf{L})_2](CF_3SO_3)_2$: *Fw* = 1206.17, 0.08 × 0.05 × 0.03 mm$^3$, monoclinic, *Pc*, *a* = 11.8459(3) Å, *b* = 19.8379(4) Å, *c* = 11.8919(3) Å, $\beta$ = 117.494(3)°, *V* = 2478.95(12) Å$^3$, *Z* = 2, *T* = 100 K, $D_{calcd}$ = 1.616 g cm$^{-3}$, $\mu$(Cu $K\alpha$) = 2.578 mm$^{-1}$, *GOF* = 1.032, $R_1(I > 2\sigma)$ = 0.0452, $wR_2$(all) = 0.1157.

Crystallographic data for $[Cu(\mathbf{L})]BPh_4$: *Fw* = 773.22, 0.11 × 0.05 × 0.02 mm$^3$, triclinic, *P–1*, *a* = 11.4008(3) Å, *b* = 11.5395(4) Å, *c* = 15.8744(6) Å, $\alpha$ = 92.725(3)°, $\beta$ = 108.344(3)°, $\gamma$ = 99.419(3)°, *V* = 1944.61(12) Å$^3$, *Z* = 2, *T* = 100 K, $D_{calcd}$ = 1.321 g cm$^{-3}$, $\mu$(Cu $K\alpha$) = 1.103 mm$^{-1}$, *GOF* = 1.022, $R_1(I > 2\sigma)$ = 0.0508, $wR_2$(all) = 0.1424.

*Theoretical Calculations*

DFT calculations on the molecular and electronic structures of $[Cu^{I}(\mathbf{L})]^+$ and $[Cu(\mathbf{L})]^{2+}$ were performed using the Gaussian 16 program suite (Revision C.02) [33]. Atomic coordinates for geometry optimization of $[Cu^{I}(\mathbf{L})]^+$ were taken from those determined by the single-crystal XRD analysis. Geometry optimization of $[Cu(\mathbf{L})]^{2+}$ was performed using the XRD determined structure of $[Cu^{I}(\mathbf{L})]^+$ as the initial geometry, while the net electric charge of +2 and spin multiplicity of doublet spin state were considered. B3LYP [34] was employed as the functional and a conductor-like polarized continuum model (dielectric constant: 35.688) was included in all calculations because this method is known to give reasonable accuracy [35]. The 6-311++G(d,p) basis sets were used. Vibrational-frequency calculations were performed at the same level of theory to confirm that no imaginary frequency was present. Single-point calculations for energetic analysis were performed on the optimized geometry using the same condition. The spin-density plots and molecular orbitals were

 doi:10.20944/preprints202508.1982.v1



visualized using GaussView 6.1 [36]. TD-DFT calculations were performed on the optimized geometry using the same conditions. Theoretical electronic transition spectra were recorded for low-lying excited states using 50 roots to generate absorption spectra for >300 nm.

## 4. Conclusions

We have demonstrated that the addition of **L** to a solution of $Cu^{II}$ induces the reduction of $Cu^{II}$ to $Cu^{I}$, with concomitant formation of $[Cu^{I}_2(\mathbf{L})_2](CF_3SO_3)_2$ and $[Cu^{I}(\mathbf{L})]BPh_4$ depending on the $Cu^{II}$ source. In acetonitrile, $[Cu^{I}(\mathbf{L})]BPh_4$ exhibits a reversible redox couple at 0.00 V vs. $Fc^{+/0}$. By combining spectroelectrochemical and EPR measurements with DFT and TD-DFT calculations, the redox equilibrium observed in $[Cu^{I}(\mathbf{L})]BPh_4$ was assigned to the $[Cu^{I/II}(\mathbf{L})]^{+/2+}$ couple. A comparison between the molecular structure of $[Cu^{II}(\mathbf{L})]^{2+}$ and those of previously reported pyridine-containing $N_4$ Schiff-base $Cu^{II}$ complexes clearly suggested that the observed reduction from $Cu^{II}$ to $Cu^{I}$ is likely driven by biphenyl-induced torsional strain in **L**. This study demonstrates that an appropriate design of the ligand structure enables the control of the complexation-induced reduction of $Cu^{II}$, providing valuable information for designing and controlling the valence isomerization of Cu complexes.

**Supplementary Materials:** The following supporting information can be downloaded at the website of this paper posted on Preprints.org, Figures S1–S6; Table S1; detailed description of screening of reaction conditions for the preparation of $[Cu(\mathbf{L})]BPh_4$.

**Author Contributions:** Dr. T.T. devised the main conceptual ideas, supervised the project, carried out all experiments and theoretical calculations, and wrote the manuscript in consultation with all co-authors. D.S., Prof. Dr. S. I., and Prof. Dr. T.O. carried out formal analyses and discussed experimental results with Dr. T.T. Dr. N.H carried out DFT calculations and discussed all experimental results with Dr. T.T. All authors have given approval to the final version of the manuscript.

**Funding:** This work was supported in part by Grants-in-Aid for Scientific Research (No. 23K19272 to T.T.) and the Sasakawa Scientific Research Grant from The Japan Science Society. The computational calculations were performed at the Research Center for Computational Science, Okazaki, Japan (Project: 23-IMS-C987, 24-IMS-C264, 25-IMS-C311).

**Data Availability Statement:** The data are contained in this article. Further reasonable inquiries can be directed to the corresponding author.

**Acknowledgments:** We thank Mr. Yoji Morifuku at the Center for Instrumental Analysis, Yamaguchi University for the single-crystal XRD measurements.

**Conflicts of Interest:** The authors declare no conflicts of interest. The funders had no role in the design of the study, in the collection, analyses, or interpretation of data, in the writing of the manuscript, or in the decision to publish the results.

## References

1. Solomon, E.I.; Heppner, D.E.; Johnston, E.M.; Ginsbach, J.W.; Cirera, J.; Qayyum, M. ; Kieber-Emmons, M.T.; Kjaergaard, C.H.; Hadt, R.G.; Tian, L. Copper active sites in biology. *Chem. Rev.* **2014**, *114*, 3659–3853.
2. Solomon, E.I.; Szilagyi, R.K.; George, S.D.; Basumallick, L. Electronic structures of metal sites in proteins and models: contributions to function in blue copper proteins. *Chem. Rev.* **2004**, *104*, 419–458.
3. Whittaker, W.J. Free radical catalysis by galactose oxidase. *Chem. Rev.* **2003**, *103*, 2347–2363.
4. Takeyama, T.; Shimazaki, Y. Diversity of oxidation state in copper complexes with phenolate ligands. *Dalton Trans.* **2024**, 53, 3911–3929.
5. Kitagawa, S.; Munakata, M.; Higashi, A. Autoreduction of copper(II) complexes of 6,6′-diakyl-2,2′-bipyridine and characterization of their copper(I) complexes. *Inorg. Chim. Acta* **1984**, *84*, 79–84.

 doi:10.20944/preprints202508.1982.v1




6. Malachowski, M.R.; Adams, M.; Elia, N.; Rheingold, A.L.; Kelly, R.S. Enforcing geometrical constraints on metal complexes using biphenyl-based ligands: spontaneous reduction of copper(II) by sulfur-containing ligands. *J. Chem. Soc. Dalton Trans.* **1999**, 2177–2182.
7. Su, C.Y.; Liao, S.; Wanner, M.; Fiedler, J.; Zhang, C.; Kang, B.S.; Kaim, W. The copper(I)/copper(II) transition in complexes with 8-alkylthioquinoline based multidentate ligands. *Dalton Trans.* **2003**, 189–202.
8. Noda, K.; Sasaki, T.; Iwatsuki, S.; Kashiwabara, K.; Suzuki, T.; Takagi, H.D. Syntheses and first structural analyses of Cu(I)–PS complexes with bidentate 1,1-diphenyl-1-phospha-4-thiapentane (mtdpp) and quadridentate 5,9-diphenyl-5,9-diphospha-2,12-dithiatridecane (2,3,2-SPPS): successful synthetic route for monomeric $[Cu(mtdpp)_2]BF_4$ and dimeric $[Cu_2(2,3,2\text{-}SPPS)_2](BF_4)_2$. *Inorg. Chim. Acta.* **2004**, *357*, 526–532.
9. Kumari, S.; Muthuramalingam, S.; Dhara, A.K.; Singh, U.P.; Mayilmurugan, R.; Ghosh, K. Cu(I) complexes obtained via spontaneous reduction of Cu(II) complexes supported by designed bidentate ligands: bioinspired Cu(I) based catalysts for aromatic hydroxylation. *Dalton Trans.* **2020**, *49*, 13829–13839.
10. Fedorova, O.A.; Shepel, N.E.; Tokarev, S.D.; Lukovskaya, E.V.; Sotnikova, Y.A.; Moiseeva, A.A.; Aleo, A.D.; Fages, F.; Maurel F.; Fedorov, Y.V. *New J. Chem.* **2019**, *43*, 2817–2827.
11. Morimoto, Y.; Inoue, K. Itoh, S. Reactivity of copper(I) complexes supported by tripodal nitrogen-containing tetradentate ligands toward gaseous diatomic molecules, NO, CO and $O_2$. *Dalton Trans.* **2025**, *54*, 5327–5333.
12. Mikata, Y.; Akedo, M.; Hamamoto, E.; Yoshida, S.; Shoji, S.; Ohsedo, Y.; Matsuo, T.; Storr, T.; Funahashi Y. Structural and electrochemical properties of mononuclear copper(II) complexes with pentadentate ethylenediamine-based ligands with pyridine/quinoline/isoquinoline/quinoxaline binding sites. *Dalton Trans.* **2024**, *53*, 16716–16732.
13. Mekhail, M.A.; Smith, K.J.; Freire, D.M.; Pota, K.; Nguyen, N.; Burnett, M.E.; Green, K.N. Increased efficiency of a functional SOD mimic achieved with pyridine modification on a pyclen-based copper(II) complex. *Inorg. Chem.* **2023**, *62*, 5415–5425.
14. Gagne, R.R.; Kreh, R.P.; Dodge, J.A.; Marsh, R.E.; McCool, M. Synthesis and structure of (*N*,*N*,*N*′,*N*′-tetrakis(2-pyridylmethyl)ethylenediamine)dicopper(I) and its dicarbonyl adduct. *Inorg. Chem.* **1982**, *21*, 254–261.
15. Siebe, L.; Butenuth, C.; Stammler, A.; Bögge, H.; Walleck, S.; Glaser, T. Generation and reactivity of μ-1,2-peroxo $Cu^{II}Cu^{II}$ and bis-μ-oxo $Cu^{III}Cu^{III}$ species and catalytic hydroxylation of benzene to phenol with hydrogen peroxide. *Inorg. Chem.* **2024**, *63*, 2627–2639.
16. Zhang, C.X.; Kaderli, S.; Costas, M.; Kim, E.; Neuhold, Y.-M.; Karlin, K. D.; Zuberbühler, A.D. Copper(I)–dioxygen reactivity of $[(L)Cu^{I}]^{+}$ (L = tris(2-pyridylmethyl)amine): kinetic/thermodynamic and spectroscopic studies concerning the formation of Cu–$O_2$ and $Cu_2$–$O_2$ adducts as a function of solvent medium and 4-pyridyl ligand substituent variations. *Inorg. Chem.* **2003**, *42*, 1807–1824.
17. Tapia, M.; Pahari, S.K.; Das, S.; Khan, F.S.T.; Hematian, S. Dimerization in TMPA-based copper(i) complexes: implications for redox kinetics and thermodynamics. *Inorg. Chem.* **2025**, *64*, 12416–12422.
18. Debnath, S.; Laxmi, S.; McCubbin Stepanic, O.; Quek, S.Y.; van Gastel, M.; DeBeer, S.; Krämer, T.; England, J. A four-coordinate end-on superoxocopper(ii) complex: probing the link between coordination number and reactivity. *J. Am. Chem. Soc.* **2024**, *146*, 23704–23716.
19. Langerman, M.; Hetterscheid, D.G.H. Fast oxygen reduction catalyzed by a copper(ii) tris(2-pyridylmethyl)amine complex through a stepwise mechanism. *Angew. Chem., Int. Ed.* **2019**, *58*, 12974–12978.
20. Wijeratne, G.B.; Hematian, S.; Siegler, M.A.; Karlin, K.D. Copper(I)/NO(g) reductive coupling producing a trans-hyponitrite bridged dicopper(II) complex: redox reversal giving copper(I)/NO(g) disproportionation. *J. Am. Chem. Soc.* **2017**, *139*, 13276–13279.
21. Amendola, V.; Fabbrizzi, L.; Gianelli, L.; Maggi, C.; Mangano, C.; Pallavicini, P.; Zema, M. Electrochemical assembling/disassembling of helicates with hysteresis. *Inorg. Chem.* **2001**, *40*, 3579–3587.
22. Takeyama, T.; Suzuki, T.; Kikuchi, M.; Kobayashi, M.; Oshita, H.; Kawashima, K.; Mori, S.; Abe, H.; Hoshino, N.; Iwatsuki, S.; Shimazaki, Y. Solid state characterization of one- and two-electron oxidized $Cu^{II}$-salen complexes with *para*-substituents: geometric structure-magnetic property relationship. *Eur. J. Inorg. Chem.* **2021**, *2021*, 4133.

 doi:10.20944/preprints202508.1982.v1




23. Kunert, R.; Philouze, C.; Berthiol, F.; Jarjayes, O.; Storr, T.; Thomas. F.; Distorted copper(II) radicals with sterically hindered salens: electronic structure and aerobic oxidation of alcohols. *Dalton Trans.* **2020**, *49*, 12990–13002.
24. Wang, Y.; DuBois, J.L.; Hedman, B.; Hodgson, K.O.; Stack, T.D.P. Catalytic galactose oxidase models: biomimetic Cu(II)-phenoxyl-radical reactivity. *Science* **1998**, *279*, 537–540.
25. Adams, H.; Bailey, N.A.; Dwyer, M.J.S. Fenton, D.E.; Hellier, P.C.; Hempstead P.D; Latour, J.M. Synthesis and crystal structure of a first-generation model for the trinuclear copper site in ascorbate oxidase and of a dinuclear silver precursor. *J. Chem. Soc., Dalton Trans.* **1993**, 1207–1216.
26. Kitajima, N.; Fujisawa, K.; Morooka, Y. Tetrahedral copper(II) complexes supported by a hindered pyrazolylborate formation of the thiolato complex, which closely mimics the spectroscopic characteristics of blue copper proteins. *J. Am. Chem. Soc.* **1990**, *112*, 3210–3212.
27. Shimizu, I.; Morimoto, Y.; Faltermeier, D.; Kerscher, M.; Paria, S.; Abe, T.; Sugimoto, H.; Fujieda, N.; Asano, K.; Suzuki, T.; Comba, P.; Itoh, S. Tetrahedral copper(II) complexes with a labile coordination site supported by a tris-tetramethylguanidinato ligand. *Inorg. Chem.* **2017**, *56*, 9634–9645.
28. Shima,Y.; Suzuki, T.; Abe, H.; Yajima, T.; Mori, S.; Shimazaki, Y. Non-innocent redox behavior of $Cu^{II}$–*p*-dimethylaminophenolate complexes: formation and characterization of the $Cu^{I}$–phenoxyl radical species. *Chem. Commun.* **2022**, *58*, 6401−6404.
29. Takeyama, T.; Tsushima S.; Takao, K. Effects of substituents on the molecular structure and redox behavior of uranyl(V/VI) complexes with $N_3O_2$-donating Schiff base ligands. *Inorg. Chem.* **2021**, *60*, 11435–11449.
30. Takeyama, T.; Tsushima, S.; Takao, K. Utility of redox-active ligands for reversible multi-electron transfer in uranyl(VI) complexes. *Inorg. Chem. Front.* **2023**, *10*, 4028–4044.
31. Sheldrick, G.M. Crystal structure refinement with SHELXL. *Acta Crystallogr. Sect. C Struct. Chem.* **2015**, *71*, 3–8.
32. Dolomanov, O.V.; Bourhis, L.J.; Gildea, R.J.; Howard, J.A.K.; Puschmann, H. *OLEX2*: a complete structure solution, refinement and analysis program. *J. Appl. Crystallogr.* **2009**, *42*, 339–341.
33. *Gaussian 16, Revision C.02*, Frisch, M.J.; Trucks, G.W.; Schlegel, H.B.; Scuseria, G.E.; Robb, M.A.; Cheeseman, J.R.; Scalmani, G.; Barone, V.; Petersson, G.A.; Nakatsuji, H.; Li, X.; Caricato, M.; Marenich, A.V.; Bloino, J.; Janesko, B.G.; Gomperts, R.; Mennucci, B.; Hratchian, H.P.; Ortiz, J.V.; Izmaylov, A.F.; Sonnenberg, J.L.; Williams-Young, D.; Ding, F.; Lipparini, F.; Egidi, F.; Goings, J.; Peng, B.; Petrone, A.; Henderson, T.; Ranasinghe, D.; Zakrzewski, V.G.; Gao, J.; Rega, N.; Zheng, G.; Liang, W.; Hada, M.; Ehara, M.; Toyota, K.; Fukuda, R.; Hasegawa, J.; Ishida, M.; Nakajima, T.; Honda, Y.; Kitao, O.; Nakai, H.; Vreven, T.; Throssell, K.; Montgomery, J.A., Jr.; Peralta, J.E.; Ogliaro, F.; Bearpark, M.J.; Heyd, J.J.; Brothers, E.N.; Kudin, K.N.; Staroverov, V.N.; Keith, T.A.; Kobayashi, R.; Normand, J.; Raghavachari, K.; Rendell, A.P.; Burant, J.C.; Iyengar, S.S.; Tomasi, J.; Cossi, M.; Millam, J.M.; Klene, M.; Adamo, C.; Cammi, R.; Ochterski, J.W.; Martin, R.L.; Morokuma, K.; Farkas, O.; Foresman, J.B.; Fox, D.J. Gaussian, Inc., Wallingford CT, 2019.
34. Lee, C.; Yang, W.; Parr, R.G. Development of the Colle-Salvetti correlation-energy formula into a functional of the electron density. *Phys. Rev. B* **1988**, *37*, 785–789.
35. Marenich, A.V.; Cramer, C.J.; Truhlar, D.G. Universal solvation model based on solute electron density and on a continuum model of the solvent defined by the bulk dielectric constant and atomic surface tensions. *J. Phys. Chem. B* **2009**, *113*, 6378–6396.
36. Dennington, R.; Keith, T.A.; Millam, J.M. *GaussView, Version 6*; Semichem Inc: Shawnee Mission, KS, 2016.